Journal of Sound and Vibration (1998) **216**(5), 865–888
Article No. sv981740

ACTIVE CONTROL OF VIBRATIONS AND NOISE OF DOUBLE WALL CYLINDRICAL SHELLS

C.-Y. WANG AND R. VAICAITIS

Department of Civil Engineering and Engineering Mechanics, Columbia University, New York, U.S.A.

(*Received* 10 *June* 1996, *and in final form* 11 *May* 1998)

Active control of vibrations and noise transmission of double wall composite cylindrical shells using pairs of spatially discrete piezoelectric actuators is investigated. The velocity feedback and sound pressure rate feedback control procedures are developed. The inner and outer shells which are separated by a soft core are modelled by Love's thin shell theory for laminate composite materials and the inputs are taken as stationary random pressures and/or random point forces. A Galerkin-like procedure is used to obtain solutions of the governing structural–acoustic equations. Parametric studies are performed to demonstrate the effect of actuator placement, actuator size, control gains, spillover, structural and acoustic damping characteristics.

1. INTRODUCTION

Active control of vibrations and noise transmission/radiation has been a growing interest for application to aircraft, space structures, automobiles, enclosures, etc. [1–23]. Rapid development of high-speed microprocessors and piezoelectric/piezoceramic materials provided alternative methods for vibration reduction and noise attenuation [24–29]. Most of the recent applications of active vibration and noise transmission/radiation control have been devoted to deterministic inputs where the phase relationships between inputs, response and control forces can be established.

We present an analytical study of active control of vibrations and noise transmission of double wall cylindrical shells to random inputs. The thin wall shells are made of fiber reinforced composite materials and the core separating the two shells is soft so that bending effects in the core can be neglected. Love's thin shell theory is used to model coupled vibrations of inner and outer shells [30, 31]. The equations of motion are solved using a Galerkin-like procedure [31]. Results are presented to illustrate the superiority of sound pressure rate feedback over the velocity feedback control for noise transmission. The differences of vibration and noise transmission control for random point force inputs and uniformly distributed sound pressure inputs are demonstrated. Parametric studies are

0022–460X/98/400865 + 24 $30.00/0

performed to show the sensitivity of actuator size, placement and voltage gain on the performance of active control.

2. THE FORMULATION OF EQUATIONS OF MOTION AND SOLUTION PROCEDURE

2.1. DOUBLE WALL CYLINDRICAL SHELL

The sandwich shell system is composed of two simply supported cylindrical shells and a soft viscoelastic core, as shown in Figure 1. Each shell is constructed from layers of fiber-reinforced laminate [30, 31]. The fibers are basically the load carriers. The orientation of fibers is defined in Figure 1 with respect to the chosen co-ordinates. The exterior shell is exposed to random loads. Two different piezoelectric element configurations, surface-bonded and embedded, are considered in this study. In Figure 2, an active piezoelectric system, where pairs of discrete piezoelectric elements are attached/embedded to inner and outer shells, is shown. The collocated piezoelectric sensors/actuators are assumed to be placed symmetrically with respect to the middle surface of each shell. The polling direction of the top and bottom piezoelectric actuators is in the same direction. However, the external electric fields are applied in opposite directions. Thus, under this action the substrate will deform in bending. Consider first surface-bonded actuators and a single shell.

By neglecting all components of rotary inertia, the equations of equilibrium are

$$\frac{\partial N_x}{\partial x} + \frac{\partial N_{x\theta}}{R\partial\theta} + f_x = m\ddot{u}, \tag{1}$$

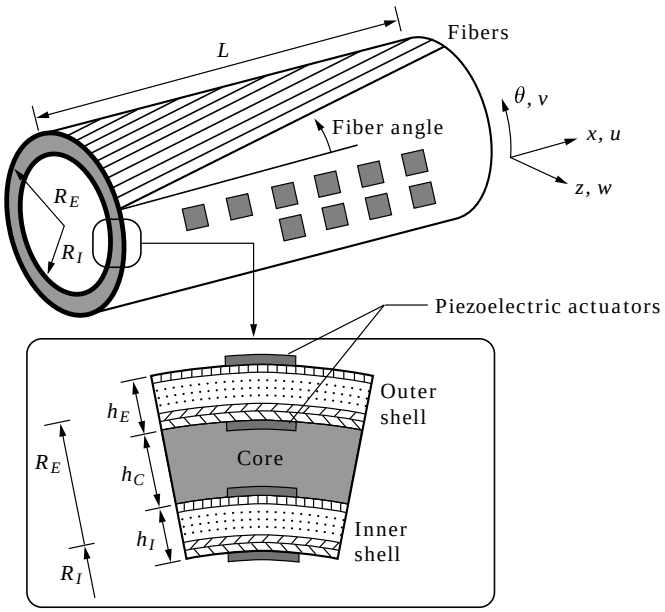

Figure 1. A double wall laminate composite circular cylindrical shell and co-ordinate system.

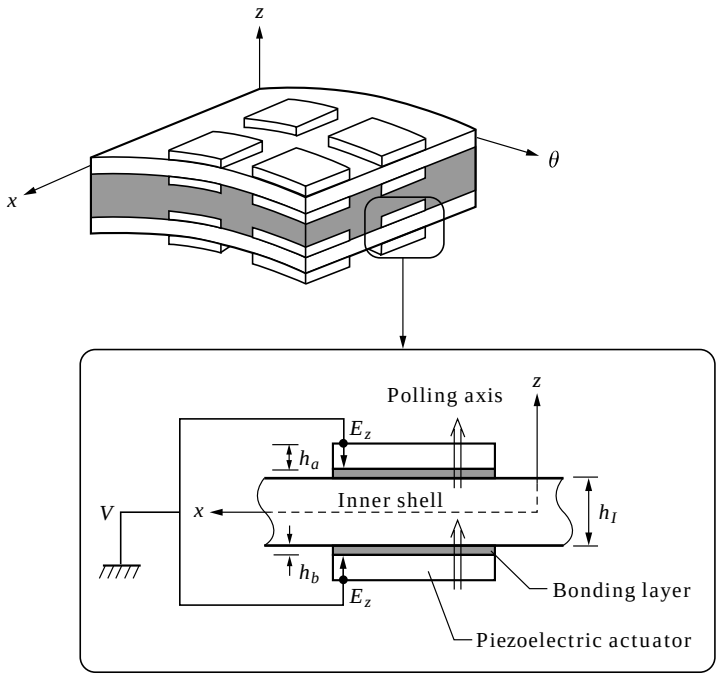

Figure 2. Actuator placement on a double wall shell construction, polling and external electric field directions.

$$\frac{\partial N_{x\theta}}{\partial x} + \frac{\partial N_\theta}{R\partial\theta} + \frac{Q_\theta}{R} + f_\theta = m\ddot{v}, \tag{2}$$

$$\frac{\partial^2 M_x}{\partial x^2} + 2\,\frac{\partial^2 M_{x\theta}}{R\partial x\partial\theta} + \frac{\partial^2 M_\theta}{R^2\partial\theta^2} - \frac{N_\theta}{R} + f_z = m\ddot{w}, \tag{3}$$

where f_x, f_θ and f_z are the components of the external loads acting on the shell and a dot indicates time derivative.

Following Love's first approximation theory of thin shells [32], the in-plane force and moment resultants in matrix form are

$$\{\mathbf{N}\} = ([A] + \chi[A^b] + \chi[A^a])\{\boldsymbol{\epsilon}\} + ([B] + \chi[B^b] + \chi[B^a])\{\boldsymbol{\kappa}\}, \tag{4}$$

$$\{\mathbf{M}\} = ([B] + \chi[B^b] + \chi[B^a])\{\boldsymbol{\epsilon}\} + ([D] + \chi[D^b] + \chi[D^a])\{\boldsymbol{\kappa}\} - \chi[M^a], \tag{5}$$

in which a and b represent the piezoelectric actuator and the bonding layer between the actuator and the shell; matrices [A], [B] and [D] are given in reference [33]. The position function $\chi(x, \theta)$ is defined as

$$\chi(x, \theta) = \begin{cases} 1, & \text{if actuators exist,} \\ 0, & \text{otherwise.} \end{cases} \tag{6}$$

The strain $\{\boldsymbol{\epsilon}\}$ and curvature change $\{\boldsymbol{\kappa}\}$ vectors are

$$\begin{Bmatrix} \epsilon_x \\ \epsilon_\theta \\ \epsilon_{x\theta} \end{Bmatrix} = \begin{Bmatrix} \dfrac{\partial u}{\partial x} \\ \dfrac{\partial v}{R\partial\theta} + \dfrac{w}{R} \\ \dfrac{\partial v}{\partial x} + \dfrac{\partial u}{R\partial\theta} \end{Bmatrix}, \qquad \begin{Bmatrix} \kappa_x \\ \kappa_\theta \\ \kappa_{x\theta} \end{Bmatrix} = \begin{Bmatrix} -\dfrac{\partial^2 u}{\partial x^2} \\ -\dfrac{\partial^2 w}{R^2\partial\theta^2} - \dfrac{1}{R}\dfrac{\partial v}{R\partial\theta} \\ -2\left(\dfrac{\partial^2 w}{R\partial x\partial\theta} + \dfrac{1}{R}\dfrac{\partial v}{\partial x}\right) \end{Bmatrix}. \quad (7)$$

The actuator induced moment vector $\{\mathbf{M}^a\}$ is

$$\{\mathbf{M}^a\} = [B^a]\begin{Bmatrix} d_{31}E_z \\ d_{32}E_z \\ 0 \end{Bmatrix}, \quad (8)$$

in which d_{31} and d_{32} are the piezoelectric strain constants, E_z is the electric field applied to the piezoelectric actuator in the z-axis direction, and $[B^a]$ is the coupling stiffness matrix. The piezoelectric strain constant matrix $[d]$ is [34]

$$[d] = \begin{bmatrix} 0 & 0 & 0 & 0 & d_{15} & 0 \\ 0 & 0 & 0 & d_{24} & 0 & 0 \\ d_{31} & d_{32} & d_{33} & 0 & 0 & 0 \end{bmatrix}. \quad (9)$$

For a thin piezoelectric patch with poling direction perpendicular to the patch, only the constants d_{31} and d_{32} are needed.

In the present study, it was assumed that external electric fields are always applied in the opposite direction to a pair of discrete actuators shown in Figure 2. Thus, for thin cylindrical shells the effect of active in-plane forces, $\{\mathbf{N}^a\}$, can be neglected. However, when polling and applied electric fields are in the same direction, in-plane forces in the circumferential direction are the dominant components for membrane action control [19–22]. Furthermore, the discrete patches of thin piezoelectric actuators distributed over both sides of inner and outer shells, shown in Figures 1 and 2, do not contribute much to the overall shell stiffness.

For a laminate composite the extensional stiffnesses A_{ij}, the extensional-bending stiffnesses B_{ij} and the bending stiffnesses D_{ij} can be obtained from [30, 31]

$$A_{ij} = \sum_{k=1}^{N} C_{ij}^{(k)}(z_{k+1} - z_k), \qquad i, j = 1, 2, 6; \quad (10)$$

$$B_{ij} = \tfrac{1}{2}\sum_{k=1}^{N} C_{ij}^{(k)}(z_{k+1}^2 - z_k^2), \qquad i, j = 1, 2, 6; \quad (11)$$

$$D_{ij} = \tfrac{1}{3}\sum_{k=1}^{N} C_{ij}^{(k)}(z_{k+1}^3 - z_k^3), \qquad i, j = 1, 2, 6; \quad (12)$$

in which $C_{ij}^{(k)}$ are the elastic constants of the kth lamina [35] and z_k, z_{k+1} are distances measured from the reference surface, as shown in Figure 1. The mass per unit area is calculated from

$$m = \sum_{k=1}^{n} \rho_k h_k + 2 \sum_{j=1}^{M} \chi(\rho_{bj} h_{bj} + \rho_{aj} h_{aj}), \tag{13}$$

in which N is the number of laminate layers and M is the number of actuators bonded to the shell surface.

The matrices $[A^a]$, $[B^a]$ and $[D^a]$ are extensional, coupling and bending stiffnesses of the piezoelectric actuators

$$[A^a] = \int_{z_a} [C^a]\,\mathrm{d}z, \qquad [B^a] = \int_{z_a} [C^a] z\,\mathrm{d}z, \qquad [D^a] = \int_{z_a} [C^a] z^2\,\mathrm{d}z, \tag{14–16}$$

in which $[C^a]$ is the elastic constant matrix of the piezoelectric actuators.

The matrices $[A^b]$, $[B^b]$ and $[D^b]$ are extensional, coupling and bending stiffness matrices of the bonding layer. These matrices can be obtained in a similar fashion as equations (14)–(16), where matrix $[C^a]$ is replaced with the elastic constant matrix $[C^b]$ of the bonding layer and integrations are across the thicknesses of the bonding layers.

For the embedded actuator configuration, the laminate substrate needs to be cut-out to accommodate the piezoelectric actuators. It is assumed that the strains developed in the actuators are compatible with the strains of the surrounding media. Furthermore, it is assumed that stiffness and mass of the laminate composite do not change by much after the installation of the embedded actuators. Thus, the force and moment resultants can be calculated from

$$\{\mathbf{N}\} = [A]\{\boldsymbol{\epsilon}\} + [B]\{\boldsymbol{\kappa}\}, \tag{17}$$

$$\{\mathbf{M}\} = [B]\{\boldsymbol{\epsilon}\} + [D]\{\boldsymbol{\kappa}\} - \chi[M^a]. \tag{18}$$

By applying equations (1)–(18) to both inner and outer shells shown in Figure 1, the equations of motion of a double wall sandwich shell system can be developed. In the present paper, the core is assumed to be soft so that bending effects in the core can be neglected. Then, the equations of motion for the external shell can be written as

$$L_{11}^E u_E + L_{12}^E v_E + L_{13}^E w_E + k_x(u_E - u_I) + f_x^E = \left(m_E + \frac{m_c}{3}\right)\ddot{u}_E + \frac{m_c}{6}\ddot{u}_I, \tag{19}$$

$$L_{21}^E u_E + L_{22}^E v_E + L_{23}^E w_E + k_\theta(v_E - v_I) + f_\theta^E + f_\theta^{aE} = \left(m_E + \frac{m_c}{3}\right)\ddot{v}_E + \frac{m_c}{6}\ddot{v}_I, \tag{20}$$

$$L_{31}^E u_E + L_{32}^E v_E + L_{33}^E w_E + k_z(w_E - w_I) + f_z^E + f_z^{aE} = \left(m_E + \frac{m_c}{3}\right)\ddot{w}_E + \frac{m_c}{6}\ddot{w}_I, \tag{21}$$

in which f_x^E, f_θ^E and f_z^E are the components of the random loads acting on the external shell, f_x^{aE} and f_x^{aE} are the components of the actuation forces produced on the external shell by piezoelectric actuators. In equations (19)–(21), k_x and k_θ are the shear spring constants, k_z is the extensional spring constant, the superscripts and subscripts of I, E and C denote the inner shell, the outer shell and the core, respectively. In the present approach, it is assumed that displacements vary linearly in the core. The terms which contain $m_c/3$ and $m_c/6$ represent the apportioned contributions of the mass of the core to both face shells. The differential operators L_{ij}^E are given in reference [33]. A similar set of equations to these, given in equations (19)–(21), can be developed for the inner shell by interchanging the superscripts and subscripts denoted by E with I.

The solution for a simply supported cylindrical shell can be written as

$$u_E(x, \theta, t) = \sum_{m=1}^{\infty} \sum_{n=0}^{\infty} \sum_{\alpha=0}^{1} U_{mn\alpha}^E(x, \theta) q_{mn\alpha}^E(t), \tag{22}$$

$$v_E(x, \theta, t) = \sum_{m=1}^{\infty} \sum_{n=0}^{\infty} \sum_{\alpha=0}^{1} V_{mn\alpha}^E(x, \theta) q_{mn\alpha}^E(t), \tag{23}$$

$$w_E(x, \theta, t) = \sum_{m=1}^{\infty} \sum_{n=0}^{\infty} \sum_{\alpha=0}^{1} W_{mn\alpha}^E(x, \theta) q_{mn\alpha}^E(t), \tag{24}$$

in which $q_{mn\alpha}^E(t)$ are the generalized co-ordinates of the outer shell, $U_{mn\alpha}^E(x, \theta)$, $V_{mn\alpha}^E(x, \theta)$ and $W_{mn\alpha}^E(x, \theta)$ are the shell modes

$$U_{mn\alpha}^E(x, \theta) = \hat{U}_{mn}^E \cos\left(\frac{m\pi x}{L}\right) \cos\left(n\theta - \alpha\frac{\pi}{2}\right), \tag{25}$$

$$V_{mn\alpha}^E(x, \theta) = \hat{V}_{mn}^E \sin\left(\frac{m\pi x}{L}\right) \sin\left(n\theta - \alpha\frac{\pi}{2}\right), \tag{26}$$

$$W_{mn\alpha}^E(x, \theta) = \hat{W}_{mn}^E \sin\left(\frac{m\pi x}{L}\right) \cos\left(n\theta - \alpha\frac{\pi}{2}\right), \tag{27}$$

where α is an adjustment index to identify the ring-type modes, and $\hat{U}_{mn}^E$, $\hat{V}_{mn}^E$ and $\hat{W}_{mn}^E$ are the modal amplitudes. Since the closed end shell considered in this paper does not show preference for the orientation of its ring-type modes, it is necessary to specify the preference to obtain a complete solution of the forced vibration problem. An index α is used for the two ring-type modes $\cos(n\theta)$ and $\sin(n\theta)$ which have the same natural frequency and modal amplitude.

The components of the actuation forces $f_\theta^{aE}(x, \theta, t)$ and $f_z^{aE}(x, \theta, t)$ are

$$f_\theta^{aE} = -\frac{1}{R_E} \frac{\partial(\chi M_\theta^{aE})}{R_E \partial\theta}, \tag{28}$$

$$f_z^{aE} = -\left\{\frac{\partial^2(\chi M_x^{aE})}{\partial x^2} + \frac{\partial^2(\chi M_\theta^{aE})}{R_E^2 \partial \theta^2}\right\}, \tag{29}$$

where M_x^{aE} and M_θ^{aE} can be obtained from equation (8). The discrete pairs of actuators shown in Figure 2 are polled in the same direction while the external electric fields are applied in opposite directions. For thin shells, this type of actuation does not produce any significant circumferential membrane force component, N_a^θ, to equation (28). However, for the general shell theory considered in the present study, some actuation force in circumferential direction is produced through moment M_θ^{aE}. If the external electric field is applied in the same direction to each pair of actuators, a control force, N_a^θ, will be induced in the circumferential direction [19–22]. However, the surface area of each pair of discrete actuators shown in Figures 1 and 2 that are distributed over the shell surface is assumed to be relatively small in comparison to the overall surface area of the shell. Thus, even for this type of control action, we should not expect that significant contributions will result in membrane control force, N_a^θ, from these small actuators. The position function $\chi(x, \theta)$ can be defined as

$$\chi(x, \theta) = \sum_{p=1}^{N_p} \{H(x - x_p^-) - H(x - x_p^+)\}\{H(\theta - \theta_p^-) - H(\theta - \theta_p^+)\}, \tag{30}$$

in which H is the unit step function, x_p^-, x_p^+, θ_p^-, θ_p^+ are the co-ordinates of the four edges of the pth actuator pair and N_p is the number of the piezoelectric actuator pairs. The first and second derivatives of the unit step function can be defined as delta and doublet functions, respectively. A doublet function can be used to represent a concentrated moment. Thus, equations (28) and (29) can be used as counteracting line moments at the edges of the piezoelectric actuators.

The governing equations of motion in terms of generalized co-ordinates $q_{mn\alpha}^E(t)$ and $q_{mn\alpha}^I(t)$ can be developed by substituting the assumed modal solution for u_E, v_E, w_E, u_I, v_I and w_I into equations (19)–(21) and using the orthogonality condition. The same procedure is repeated for the governing equations of the interior shell. Damping can be introduced by simply replacing the elastic constants C_{ij}^E in equations (10)–(12) by the complex elastic constants of the form $C_{ij}^E(1 + \mathrm{j}\eta_{ij}^E)$, where η_{ij}^E are the damping factors of the composite material. Damping could also be introduced in the soft core by replacing the constants k_x, k_θ and k_z with $k_x(1 + \mathrm{j}\eta_x)$, $k_\theta(1 + \mathrm{j}\eta_\theta)$ and $k_z(1 + \mathrm{j}\eta_z)$, respectively, where η_x, η_θ and η_z are the damping coefficients of the core material.

The generalized forces corresponding to the actuating forces are obtained from

$$F_{mn\alpha}^{aE}(t) = \int_0^L \int_0^{2\pi} (f_\theta^{aE} V_{mn\alpha}^E + f_z^{aE} W_{mn\alpha}^E)\, \mathrm{d}x\, R_E\, \mathrm{d}\theta, \tag{31}$$

in which R_E is the shell radius referenced to the shell layer to which the actuator is laminated. The actuation terms f_θ^{aE} and f_z^{aE} are functions of the actuator induced

moments M_x^{aE} and M_θ^{aE}. These moments can be obtained from equation (8). For a uniformly distributed electric field,

$$E_z^p = \frac{V_z^p}{h_a^p}, \tag{32}$$

in which V_z^{pE} and h_a^{pE} are the applied voltage and thickness of the pth piezoelectric actuator. From equation (31), the actuating generalized forces can be written as

$$F_{mn\alpha}^{aE}(t) = \sum_{p=1}^{N_p^E} Q_{mn\alpha}^{pE} V_z^p(t), \tag{33}$$

where

$$Q_{mn\alpha}^{pE} = \begin{cases} (B_{11}^a d_{31} + B_{12}^a d_{32})_p \left(\dfrac{1}{h_a^p}\right)\left(\dfrac{2m\pi L_\theta^p}{L}\right) \sin\left(\dfrac{m\pi L_x^p}{2L}\right) W_{mn\alpha}^E(x_p, \theta_p), & \text{if} \quad n = 0; \\ \left[(B_{11}^{\mathrm{a}} d_{31} B_{12}^{\mathrm{a}} d_{32})_{\mathrm{p}} \left(\dfrac{4m\pi R_E}{nL}\right) \right. \\ \quad \left. + (B_{12}^{\mathrm{a}} d_{31} + B_{22}^{\mathrm{a}} d_{32})_{\mathrm{p}} \left(\dfrac{4nL}{m\pi R_E}\right)\left(1 + \dfrac{\hat{V}_{mn\alpha}^E}{n\hat{W}_{mn\alpha}^E}\right) \right] \\ \quad \times \left(\dfrac{1}{h_a^p}\right) \sin\left(\dfrac{m\pi L_x^p}{2L}\right) \sin\left(\dfrac{nL_\theta^p}{2R_E}\right) W_{mn\alpha}^E(x_p, \theta_p), & \text{otherwise;} \end{cases} \tag{34}$$

in which L_x^p and L_θ^p are the lengths of the pth actuator pair in the longitudinal and circumferential directions, and (x_p, θ_p) denotes the local co-ordinates of the pth actuator.

The inputs to the double wall shell considered in this study are random point loads and uniformly distributed random pressure. Thus, response solutions in the form of spectral densities need to be developed. Taking the Fourier transformation on the time variable of the governing equations of motion and using random process theory [36], the response spectral densities of the transverse displacement of the inner and the outer shells are

$$S_{ww}^I(x, \theta, \omega) = \sum_{m=1}^{\infty} \sum_{n=0}^{\infty} \sum_{\alpha=0}^{1} \sum_{r=1}^{\infty} \sum_{s=0}^{\infty} \sum_{\beta=0}^{1} \{ (I_{(mn\alpha)(rs\beta)}^I H_{mn\alpha}^I H_{rs\beta}^{I*} + I_{(mn\alpha)}^E H_{mn\alpha}^{IE} H_{rs\beta}^{IE*}) W_{mn\alpha}^I W_{rs\beta}^I \}, \tag{35}$$

$$S_{ww}^E(x, \theta, \omega) = \sum_{m=1}^{\infty} \sum_{n=0}^{\infty} \sum_{\alpha=0}^{1} \sum_{r=1}^{\infty} \sum_{s=0}^{\infty} \sum_{\beta=0}^{1} \{ (I_{(mn\alpha)(rs\beta)}^E H_{mn\alpha}^E H_{rs\beta}^{E*} + I_{(mn\alpha)(rs\beta)}^I H_{mn\alpha}^{E1} H_{rs\beta}^{EI*}) W_{mn\alpha}^E W_{rs\beta}^E \}, \tag{36}$$

in which $H^I_{mn\alpha}(\omega)$ and $H^E_{mn\alpha}(\omega)$ are the frequency response functions of the inner and the outer shell, $H^{IE}_{mn\alpha}(\omega)$ and $H^{EI}_{mn\alpha}(\omega)$ are the cross-terms of the frequency response functions, an asterisk denotes a conjugate quantity, $I^I_{(mn\alpha)(rs\beta)}(\omega)$ and $I^E_{(mn\alpha)(rs\beta)}(\omega)$ are the cross-spectral densities of the generalized random input forces. If the random inputs to the inner shell are zero, equations (35) and (36) can be simplified by setting $I^I_{(mn\alpha)(rs\beta)}(\omega) = 0$. The expressions for the frequency response functions and generalized random forces are very lengthy and they are not presented in this paper. However, these expressions can be found in reference [33].

2.2. NOISE TRANSMISSION INTO A CYLINDRICAL SHELL

After the response spectral densities of shell vibrations are known, the noise transmitted through the double wall shell system can be obtained. The flexible shell is supported by rigid end caps forming a closed cylindrical enclosure. It is assumed that noise is only transmitted through the elastic shell and the entire surface of the acoustic enclosure is absorbent.

The acoustic pressure p inside the cylindrical enclosure satisfies the wave equation [31]

$$\nabla^2 p = \frac{1}{c_0^2}\ddot{p} + \beta\dot{p}, \tag{37}$$

where c_0 is the speed of sound, β is the acoustic damping coefficient and

$$\nabla^2 = \frac{\partial^2}{\partial r^2} + \frac{1}{r}\frac{\partial}{\partial r} + \frac{1}{r^2}\frac{\partial^2}{\partial \theta^2} + \frac{\partial^2}{\partial x^2}. \tag{38}$$

The boundary conditions to be satisfied by equation (37) are

$$\frac{\partial p}{\partial r} = -\rho_0 \ddot{w}_I - \frac{\rho_0}{Z_A}\dot{p}, \qquad \text{on} \quad r = R_I; \tag{39}$$

$$\frac{\partial p}{\partial x} = +\frac{\rho_0}{Z_A}\dot{p}, \qquad \text{on} \quad x = 0; \tag{40}$$

$$\frac{\partial p}{\partial x} = -\frac{\rho_0}{Z_A}\dot{p}, \qquad \text{on} \quad x = L; \tag{41}$$

in which ρ_0 is the air density inside the enclosure and Z_A is the frequency dependent acoustic point impedance of the acoustic absorbent material [37, 38].

Solving equation (37) for hard wall boundary conditions, i.e., $\partial p/\partial r = 0$ at $r = R_I$ and $\partial p/\partial x = 0$ at $x = 0$ and L, the acoustic modes of the cylindrical enclosures are

$$\Psi_{ijk\mu}(x, \theta, r) = \cos\left(\frac{i\pi x}{L}\right)\cos\left(j\theta - \mu\frac{\pi}{2}\right)\mathrm{J}_j\left(\frac{\lambda_{jk} r}{R_I}\right), \tag{42}$$

in which J_j is the Bessel function of the first kind of order j and λ_{jk} are the values of the kth zero of the first derivative of J_j, i.e., $\{\mathrm{d}[\mathrm{J}_j(r)]/\mathrm{d}r\}_{r=\lambda_{jk}} = 0$. The solution for interior acoustic pressure can be obtained by expanding the pressure in terms of acoustic modes given in equation (42) and satisfying equation (37) by a

Galerkin-like procedure. Furthermore, applying Green's second identity [39], the homogeneous acoustic equation with non-homogeneous boundary conditions can be transformed into a non-homogeneous equation with homogeneous boundary conditions. Then, the acoustic modal equations can be written as

$$\ddot{P}_{ijk\mu} + \left(2\xi^A_{ijk}\omega^A_{ijk} + \frac{\rho_0 c_0^2 A_{ijk\mu}}{Z_A V_{ijk\mu}}\right)\dot{P}_{ijk\mu} + \omega^{A^2}_{ijk} P_{ijk\mu}$$

$$= -\frac{\rho_0 c_0^2}{V_{ijk\mu}} \sum_{m=1}^{\infty} \sum_{n=0}^{\infty} \sum_{\alpha=0}^{1} B_{(mn\alpha)(ijk\mu)} \ddot{q}_{mn\alpha}, \tag{43}$$

in which ξ^A_{ijk} are the acoustic modal damping coefficients and ω^A_{ijk} are the acoustic modal frequencies

$$\omega^A_{ijk} = c_0 \sqrt{\left(\frac{i\pi}{L}\right)^2 + \left(\frac{\lambda_{jk}}{R_I}\right)^2}. \tag{44}$$

The acoustic–structural coupling coefficients $B_{(mn\alpha)(ijk\mu)}$ are

$$B_{(mn\alpha)(ijk\mu)} = \begin{cases} \dfrac{2m\epsilon_n \delta_{nj}\delta_{\alpha\mu}}{m^2 - i^2} \hat{W}^I_{mn\alpha} \mathrm{J}_j(\lambda_{jk}) R_I L, & \text{if } (m-i) \text{ odd}, \\ 0, & \text{otherwise}, \end{cases} \tag{45}$$

in which $\epsilon_n = 2$ for $n = 0$, $\epsilon_n = 1$ for $n \neq 0$; $\delta_{nj} = 1$ for $n = j$ and $\delta_{nj} = 0$ for $n \neq j$. The coefficients $V_{ijk\mu}$ and $A_{ijk\mu}$ can be obtained from

$$V_{ijk\mu} = \int_0^L \int_0^{2\pi} \int_0^{R_I} \Psi^2_{ijk\mu}(x, \theta, r)\, \mathrm{d}x R_I\, \mathrm{d}\theta\, \mathrm{d}r, \tag{46}$$

$$A_{ijk\mu} = \int_0^L \int_0^{2\pi} \Psi^2_{ijk\mu}(x, \theta, R_I)\, \mathrm{d}x\, R_I\, \mathrm{d}\theta$$

$$+ \int_0^{2\pi} \int_0^{R_I} \{\Psi^2_{ijk\mu}(0, \theta, r) + \Psi^2_{ijk\mu}(L, \theta, r)\} R_I\, \mathrm{d}\theta\, \mathrm{d}r. \tag{47}$$

Then, taking the Fourier transformation of equation (43) and using the theory of random processes [36], the spectral density of the acoustic pressure inside the cylindrical enclosure is

$$S_{pp}(x, \theta, r, \omega) = \sum_{i=0}^{\infty} \sum_{j=0}^{\infty} \sum_{k=0}^{\infty} \sum_{\mu=0}^{1} \sum_{a=0}^{\infty} \sum_{b=0}^{\infty} \sum_{c=0}^{\infty} \sum_{v=0}^{1} L_{(ijk\mu)(abcv)} H_{ijk\mu} H^*_{abcv} \Psi_{ijk\mu} \Psi_{abcv}, \tag{48}$$

in which $H_{ijk\mu}(\omega)$ are the acoustic modal frequency response functions of the cavity and can be obtained from

$$H_{ijk\mu}(\omega) = \frac{-(\rho_0 c_0^2 / V_{ijk\mu})}{\omega_{ijk}^{A^2} - \omega^2 + \mathrm{j}\omega(2\xi_{ijk}^A \omega_{ijk}^A + (\rho_0 c_0^2 A_{ijk\mu}/Z_A V_{ijk\mu}))}. \tag{49}$$

The terms $L_{(ijk\mu)(abcv)}(\omega)$ involving the acoustic–structural coupling are

$$L_{(ijk\mu)(abcv)}(\omega) = \sum_{m=1}^{\infty}\sum_{n=0}^{\infty}\sum_{\alpha=0}^{1}\sum_{r=1}^{\infty}\sum_{s=0}^{\infty}\sum_{\beta=0}^{1}\{I^I_{(mn\alpha)(rs\beta)} H^I_{mn\alpha} H^{I*}_{rs\beta}$$

$$+ I^E_{(mn\alpha)(rs\beta)} H^{IE}_{mn\alpha} H^{IE*}_{rs\beta}\} B_{(mn\alpha)(ijk\mu)} B_{(rs\beta)(abcv)}, \tag{50}$$

in which $I^E_{(mn\alpha)(rs\beta)}$ and $I^I_{(mna\alpha)(rs\beta)}$ are the cross-spectral densities of the generalized random forces of the inner and outer shells and are given in reference [33].

After the spectral density of the interior acoustic pressure is known, the band-filtered sound pressure levels (SPL) and the Sound Pressure Level (SPL) can be calculated from

$$\mathrm{SPL}(x, \theta, \omega) = 10 \log \frac{S_{pp}(x, \theta, r, \omega)\Delta\omega}{p_{ref}^2}, \qquad \mathrm{dB}, \tag{51}$$

$$\mathrm{SPL}(x, \theta) = 10 \log \frac{\int_0^{\omega_u} S_{pp}(x, \theta, r, \omega)\, \mathrm{d}\omega}{p_{ref}^2}, \qquad \mathrm{dB}, \tag{52}$$

in which p_{ref} is the reference sound pressure, $p_{ref} = 20\ \mu\mathrm{Pa}$ for airborne sound, $\Delta\omega$ is the selected frequency bandwidth, and ω_u is the upper cut-off frequency.

3. ACTIVE CONTROL OF VIBRATIONS AND NOISE TRANSMISSION

The application of active control to vibration suppression and noise transmission attenuation is aimed to large-scaled shells and wide-band random inputs. Thus, a large number of sensors/actuators will be needed to obtain the required solutions. The control scheme is designated to be multiple independent single-input/single-output feedback controllers. Two active control mechanisms are considered in this paper: direct velocity feedback and sound pressure rate feedback [23].

3.1. VELOCITY FEEDBACK

For the velocity feedback control, the shell transverse velocity measured at location (x_p, θ_p) is inverted and fed to the pth piezoelectric actuator pair as voltage with a control gain G_p^E. Then, the voltage can be written as

$$V_z^{pE}(t) = -G_p^E \dot{w}_E(x_p, \theta_p, t) = -G_p^E \sum_{m=1}^{\infty}\sum_{n=0}^{\infty}\sum_{\alpha=0}^{1} W^E_{mn\alpha}(x_p, \theta_p)\dot{q}^E_{mn\alpha}(t). \tag{53}$$

It can be shown that active modal damping factors $\zeta^a_{mn\alpha}$ are

$$\zeta^E_{mn\alpha} = \sum_{p=1}^{N^E_p} G^E_p Q^{pE}_{mn\alpha} W^E_{mn\alpha}(x_p, \theta_p). \tag{54}$$

For collocated sensors/actuators, the active modal damping factor given in equation (54) can be incorporated as positive damping into the governing equations of shell vibrations and response spectral densities. A similar expression of the active modal damping factor can be obtained for the inner shell. Thus, the random vibration response of the double wall shell system is reduced due to increase in system damping from piezoelectric actuators.

3.2. SOUND PRESSURE RATE FEEDBACK

The direct velocity feedback control developed in section 3.1. is aimed at reducing vibrations of the double wall shell system. However, for cases where the acoustic resonances dominate the interior noise, velocity feedback might not be effective in reducing noise transmission to acceptable levels. The active control by sound pressure rate feedback could provide additional acoustic damping thereby suppressing the acoustic resonances [23]. This can be achieved by making the applied voltage to the piezoelectric actuators proportional to the sound pressure rate inside the cavity as

$$V^p_z(t) = G_p \dot{p}(x_p, \theta_p, r_p, t) = G_p \sum_{i=1}^{\infty} \sum_{j=0}^{\infty} \sum_{k=0}^{\infty} \sum_{\mu=0}^{1} \Psi_{ijk\mu}(x_p, \theta_p, r_p) \dot{P}_{ijk\mu}(t). \tag{55}$$

Substituting the above expression into equation (33) and solving the governing equations for double wall shell vibrations which contain piezoelectric actuators, the active acoustic damping factors $\zeta_{ijk\mu}$ can be obtained:

$$\zeta_{ijk\mu} = -\left\{ \sum_{p=1}^{N^I_{pz}} G^I_p \Psi_{ijk\mu}(x^I_p, \theta^I_p, r^I_p) \sum_{m=1}^{\infty} \sum_{n=0}^{\infty} \sum_{\alpha=0}^{1} (Q^p_{mn\alpha})^I H^I_{mn\alpha} B_{(mn\alpha)(ijk\mu)} \right.$$

$$\left. + \sum_{p=1}^{N^E_{pz}} G^E_p \Psi_{ijk\mu}(x^E_p, \theta^E_p, r^E_p) \sum_{m=1}^{\infty} \sum_{n=0}^{\infty} \sum_{\alpha=0}^{1} (Q^p_{mn\alpha})^E H^{IE}_{mn\alpha} B_{(mn\alpha)(ijk\mu)} \right\}. \tag{56}$$

Then, the active acoustic damping effect enters equation (43) and subsequently equation (49) as an additional $\omega^2 \zeta_{ijk\mu}$ damping term multiplied by $\dot{P}_{ijk\mu}$. Unlike the direct velocity feedback scheme, the sound pressure rate feedback does not guarantee that active damping factors $\zeta_{ijk\mu}$ will be positive. Positive damping can be guaranteed by using appropriate filters for control gain G^E_p and G^I_p.

4. NUMERICAL RESULTS

Numerical results are obtained for uniformly distributed random pressure and for random point loads acting on the exterior shell. The random pressure is taken as homogeneous truncated Gaussian white noise for which the spectral density is

$$\Phi_z^E = \begin{cases} S_0, & \text{for } 0 \leqslant f \leqslant f_u, \\ 0, & \text{otherwise,} \end{cases} \tag{57}$$

in which S_0 is a selected parameter to represent different random pressure loadings, f is the frequency and f_u is the upper cut-off frequency. For example, $S_0 = 40$ Pa^2/Hz for sound pressure level input of 110 dB and 140 dB overall level when $f_u = 1000$ Hz. The random point loads are represented by two independent random forces acting on the exterior shell, as shown in Figure 3. The spectral densities of these point forces are also taken as truncated Gaussian white noise with the spectral density

$$\Phi_z^E = \sum_{i=1}^{2} S_i \delta(x - x_i) \frac{1}{R_E} \delta(\theta - \theta_i), \tag{58}$$

in which δ denotes a delta function. Numerical results are obtained for

$$S_1 = S_2 = \begin{cases} 10 \text{ N}^2/\text{Hz}, & \text{for} \quad 0 \leqslant f \leqslant f_u, \\ 0, & \text{otherwise.} \end{cases} \tag{59}$$

For an upper frequency cut-off of 1000 Hz, the root-mean-square value of each input force is 100 N.

The dimensions of a double wall cylindrical shell shown in Figure 1 are: $L =$ 6 m, $R_I = 1{\cdot}6$ m, $R_E = 1{\cdot}65$ m, $h_c = 50$ mm, $h_I = 2{\cdot}5$ mm, and $h_E = 2$ mm. The inner and outer shells consist of ten and eight layers of multi-directional T300/N5208 Graphite/Epoxy laminate with the material properties: $E_1 =$ 181 GPa, $E_2 = 10{\cdot}3$ GPa, $G_{12} = 7{\cdot}17$ GPa, $\nu_{12} = 0{\cdot}28$, and $\rho = 1600$ kg/m^3. Each lamina has a thickness of 0·25 mm and stacking sequences starting from the bottom layer are [0°/45°/90°/–45°/90°/90°/–45°/90°/45°/0°] for the inner shell and

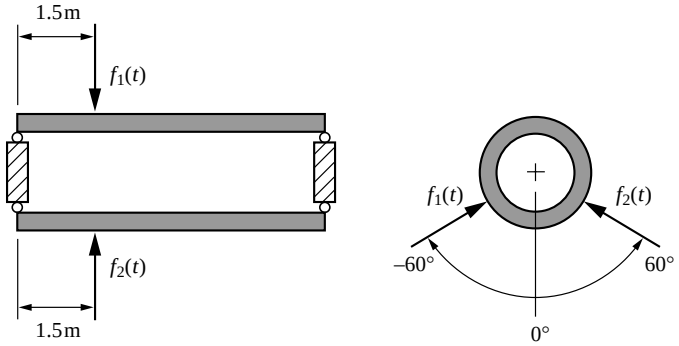

Figure 3. Locations of the point loads.

TABLE 1

Empirical constants for glass fiber materials [38]

$\Lambda_x = 0{\cdot}025$	a_1	a_2	a_3	a_4	b_1	b_2	b_3	b_4
$\Lambda \leqslant \Lambda_x$	0·396	0·135	0·0668	0·196	0·458	0·646	0·707	0·549
$\Lambda \geqslant \Lambda_x$	0·179	0·102	0·0235	0·0875	0·674	0·705	0·887	0·770

[0°/45°/–45°/90°/90°/–45°/45°/0°] for the outer shell. The damping factors of the shells and the core are taken as $\eta^I_{mn\alpha} = \eta^E_{mn\alpha} = 0{\cdot}02$ and $\eta^C_{mn\alpha} = 0{\cdot}1$, respectively.

The vibrations of a double wall shells system with a relatively soft core include flexural (in-phase) and dilatational (out-of-phase) motions [31]. The numerical results were obtained including all the modes for the selected frequency range of 0–1000 Hz. To cover this frequency range, 9940 structural modes (4970 flexural and 4970 dilatational) with $m = 1, 2, \ldots, 70$ and $n = 0, 1, \ldots, 70$, are needed. For convenience, the displacement level DL is defined as

$$\mathrm{DL} = 10 \log \frac{S_{ww}(x, \theta, f)\Delta f}{h^2}, \qquad \mathrm{dB}, \tag{60}$$

in which S_{ww} is the displacement response spectral density of either the inner or outer shell and h is the respective shell thickness.

The normal acoustic point impedance Z_A of the sound absorbing materials at the inner shell surface and the end caps can be taken as [37]

$$Z_A = \frac{Z_a}{\tanh(\Gamma_a d)}, \tag{61}$$

in which d is the thickness of the sound absorbing acoustic material, and Z_a and Γ_a are the characteristic impedance and propagation constant [38]:

$$Z_a = Z_0\{1 + a_1\Lambda^{-b_1} - \mathrm{j}a_2\Lambda^{-b_2}\}, \qquad \Gamma_a = k_0\{a_3\Lambda^{-b_3} + \mathrm{j}(1 + a_4\Lambda^{-b_4})\}, \tag{62, 63}$$

in which $Z_0 = \rho_0 c_0$ is the air characteristic impedance, $k_0 = \omega/c_0$ is the acoustic air wave number, $\Lambda = \rho_0 f/R_f$, R_f is the flow resistivity, and a_1, a_2, a_3, a_4, b_1, b_2, b_3, b_4 are empirical constants. Noise transmission is calculated for $d = 12{\cdot}5$ mm glass fiber blanket with $R_f = 18{\cdot}4\ \mathrm{kN \cdot s/m^4}$ and for empirical constants given in Table 1. The acoustic modal damping coefficients $\xi^A_{ijk\mu}$ in equations (43) and (49) were set equal to zero. Numerical results were obtained using all acoustic modes in the frequency range of 0–1000 Hz.

The displacement levels and root-mean-square displacements at $x = 3$ m and $\theta = 90°$ are shown in Figures 4 and 5 for uniform random pressure and random point force inputs. These results are for the cases without active vibration control. For a uniformly loaded shell, only the modes with $n = 0$ and odd m are excited. The peaks in Figure 4 are the breathing flexural and dilatational modes for $n = 0$. Thus, the response in the low frequency range is very low since there are no modes excited in this frequency range. For point force inputs, the shell response is dominated by low frequency modes and a large number of modes are excited. Thus, the effectiveness of active vibration control by piezoelectric actuators could

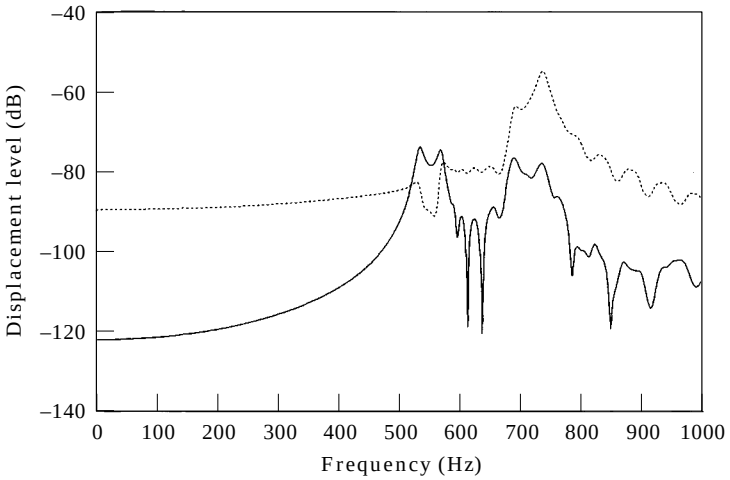

Figure 4. Displacement levels at $x = 3$ m for uniform random pressure with SPL = 110 dB: ——, inner shell, rms $w_I/h_I = 0{\cdot}00155$; ····· , outer shell, rms $w_E/h_E = 0{\cdot}00988$.

be significantly different for these two types of inputs. Different active control designs might be required to accommodate distinctly different inputs.

A wide variety of piezoelectric materials is available. Since the structure selected in this study is of large-scale and is relatively stiff, the major concern is the limitation of the actuation ability of these materials. Piezoelectric actuators with high modulus, large piezoelectric strain constant, and large applied electric field can achieve significant actuation capability. Numerical results are obtained for the following geometric and material properties of the piezoelectric actuators: $E_a = 63$ GPa, $\rho_a = 7650$ kg/m^3, $v_a = 0{\cdot}3$, $d_{31} = d_{32} = -180 \times 10^{-12}$ m/V, $L_x^p = 60$ mm, $L_\theta^p = 60$ mm, and $h_a = 1$ mm. The adhesive used for bonding actuators is assumed to be isotropic with the following properties: $E_b = 10$ GPa,

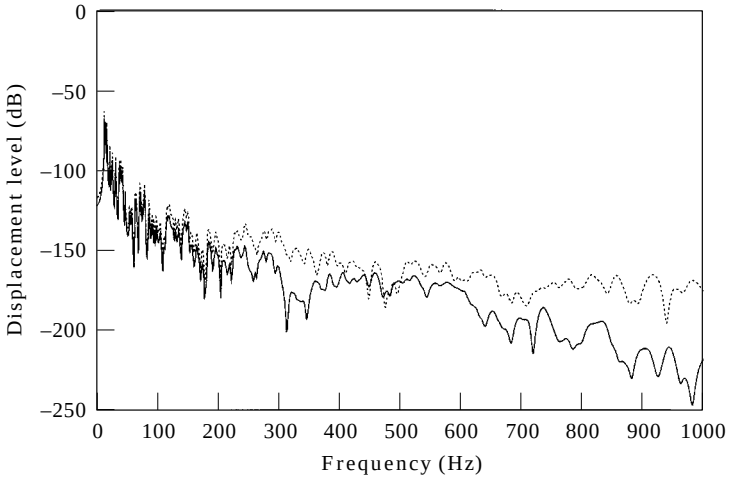

Figure 5. Displacement levels at $x = 3$ m and $\theta = 90^\circ$ for two concentrated forces: ——, inner shell, rms $w_I/h_I = 0{\cdot}06134$; ·····, outer shell, rms $w_E/h_E = 0{\cdot}07776$.

TABLE 2

The spatial-average response of controlled double wall sandwich shells with various arrangements of piezoelectric actuators for uniform pressure and point force inputs

	Uniform pressure			Point forces		
Control	$(w^I_{\text{avg}}/h_I)_{\text{rms}}$	$(w^E_{\text{avg}}/h_E)_{\text{rms}}$	SPL_{avg} (dB)	$(w^I_{\text{avg}}/h_I)_{\text{rms}}$	$(w^E_{\text{avg}}/h_E)_{\text{rms}}$	SPL_{avg} (dB)
None	0·00180	0·00767	119·6	0·0531	0·0680	116·1
Inner shell	0·00144	0·00775	118·7	0·0154	0·0215	113·5
Outer shell	0·00195	0·00715	122·0	0·0446	0·0572	116·1
Both shells	0·00158	0·00724	119·8	0·0115	0·0151	112·5

$\rho_b = 1000\ \text{kg/m}^3$, $v_b = 0{\cdot}33$, and $h_b = 0{\cdot}1$ mm. In addition, numerical results were also obtained for several different sizes of piezoelectric actuators.

To control shell vibrations and noise transmission, 270 pairs of actuators on the inner shell and 270 pairs of actuators on the outer shell were used. The actuators were arranged on the shell surface as follows: a total of 15 actuator rings are distributed longitudinally at 0·25-m intervals in the space from $x = 1{\cdot}25$ m to $x = 4{\cdot}75$ m, where each ring contains 18 actuators uniformly distributed around the circumference.

Local vibration response and local interior noise pressure could vary significantly from one location to another. To evaluate the feasibility of active vibration and noise transmission control, it is more meaningful to define spatial average quantities in terms of spectral densities, root-mean-square values, and overall noise levels. The spatial average spectral densities are defined as

$$S^L_{\text{avg}}(f) = \frac{1}{2\pi R_I L}\int_0^L \int_0^{2\pi} S^I_{ww}(x, \theta, f)\, \mathrm{d}x\, R_I\, \mathrm{d}\theta, \tag{64}$$

$$S^E_{\text{avg}}(f) = \frac{1}{2\pi R_E L}\int_0^L \int_0^{2\pi} S^E_{ww}(x, \theta, f)\, \mathrm{d}x\, R_E\, \mathrm{d}\theta, \tag{65}$$

$$S^P_{\text{avg}}(f) = \frac{1}{\pi R_I^2 L}\int_0^L \int_0^{2\pi} \int_0^{R_I} S_{pp}(x, \theta, r, f)\, \mathrm{d}x\, R_I\, \mathrm{d}\theta\, \mathrm{d}r. \tag{66}$$

The spatial-average root-mean-square vibration response and overall sound pressure levels are given in Table 2 for various velocity feedback control arrangements. The inputs are 110 dB uniform pressure and two point loads with spectral densities prescribed in equations (58) and (59). The control gains of the piezoelectric actuators are all set to $G = 5 \times 10^3$. These results indicate that active control is most effective when piezoelectric actuators are installed either on both shells or only on the inner shell. Installing piezoelectric actuators only on the outer shell could reduce vibrations of the outer shell, but has almost no effect on noise transmission. Since the vibrations of both shells are coupled, controlling vibrations of one shell might not always guarantee the best results.

TABLE 3

The spatial-average response of inner shell control with various sizes of piezoelectric actuators for uniform pressure and point force inputs

Actuator size	Uniform pressure			Point forces		
	$(w^I_{avg}/h_I)_{rms}$	$(w^E_{avg}/h_E)_{rms}$	SPL_{avg} (dB)	$(w^I_{avg}/h_I)_{rms}$	$(w^E_{avg}/h_E)_{rms}$	SPL_{avg} (dB)
None	0·00180	0·00767	119·6	0·0531	0·0680	116·1
80 × 80 mm	0·00144	0·00775	118·7	0·0154	0·0215	113·5
160 × 160 mm	0·00092	0·00790	112·9	0·0078	0·0143	109·7
240 × 240 mm	0·00060	0·00803	109·9	0·0051	0·0136	106·5

The effect of using different sizes of piezoelectric actuators is demonstrated in Table 3. In this case, the actuators are only located on the inner shell. These results indicate that for the chosen shell geometry, increasing piezoelectric actuators' size can result in greater reduction of average inner shell response and average interior noise. However, these observations should not be generalized since the effectiveness of active control depends on many parameters and not just the size of actuators. Furthermore, there are some practical limitations in the size of a discrete piezoelectric patch. The large size of the piezoelectric patch may not be commercially available. Furthermore, induced strains in piezoelectric actuators are assumed to be constant. For a large size actuator, the resonant frequency of the actuator may be close to the selected upper bound frequency range. Thus, induced strains are no longer constant [40]. In addition, the large size piezoelectric actuator may cause spillovers to the higher modes. The spillover is demonstrated in Figures 6 and 7. These results were obtained using 9940 structural modes. The spillover phenomena can be observed from the active damping factor given in equation (54).

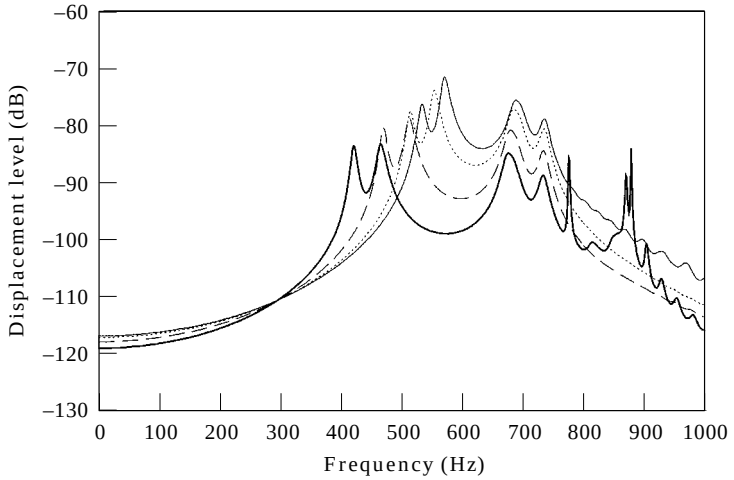

Figure 6. The inner shell spatial-average response under inner shell control for various sizes of piezoelectric actuators and uniform pressure: ——, no control; ·····, 80 × 80 mm; - - -, 160 × 160 mm; ——, 240 × 240 mm.

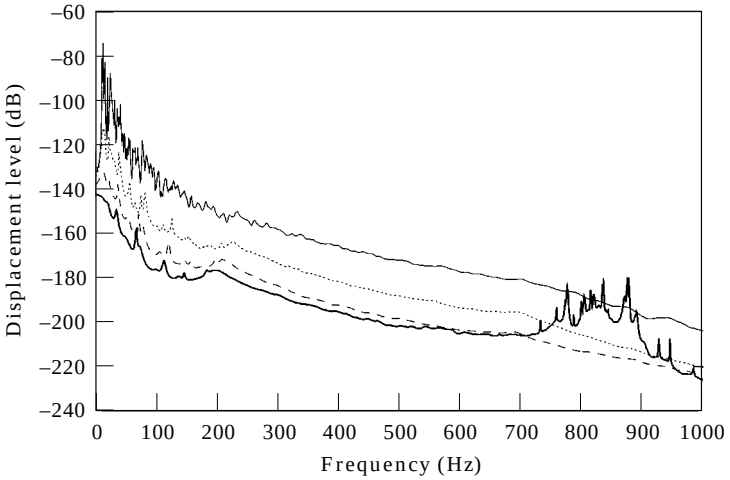

Figure 7. The inner shell spatial-average response under inner shell control for various sizes of piezoelectric actuators for point force inputs: ——, no control; ·····, 80×80 mm; - - -, 160×160 mm; ——, 240×240 mm.

The parameters in this expression are all positive except for modal terms $\sin(m\pi L_x^p/2L)$ and $\sin(nL_\theta^p/2R)$. For large values of L_x^p and L_θ^p, these terms could become negative yielding negative active damping factors which cause the spillover effect. For patch sizes satisfying $mL_x^2/2L \leqslant 1$ and $nL_\theta^p/2R_E \leqslant \pi$, active damping coefficients in equation (54) are all positive and no spillover to higher modes occurs. Thus, patch sizes could be tailored to accommodate different shell geometries with no spillover for the selected frequency range. The effect of spillover may not be very significant at higher frequencies since higher-frequency modes tend to have lower amplitudes and are more effected by damping.

The active damping factor in equation (54) is a function of control gain G. To investigate the effect of control gain, four different cases have been considered. In each case, a total of 270 pairs of piezoelectric actuators size 80×80 mm are attached only to the inner shell. The results are given in Table 4. The results for $G = 0$ correspond to the case where actuators are mounted to the inner shell but no voltage is applied to the actuators. Only the structural dynamic characteristics

TABLE 4

The spatial-average response of inner shell control with various control gains for uniform pressure and point force inputs

Control gain	Uniform pressure			Point forces		
	$(w^I_{\text{avg}}/h_I)_{\text{rms}}$	$(w^E_{\text{avg}}/h_E)_{\text{rms}}$	SPL_{avg} (dB)	$(w^I_{\text{avg}}/h_I)_{\text{rms}}$	$(w^E_{\text{avg}}/h_E)_{\text{rms}}$	SPL_{avg} (dB)
None	0·00180	0·00767	119·6	0·0531	0·0680	116·1
$G = 0$	0·00152	0·00777	119·3	0·0405	0·0528	114·9
$G = 5 \times 10^3$	0·00144	0·00775	118·7	0·0154	0·0215	113·5
$G = 5 \times 10^4$	0·00126	0·00769	116·9	0·0053	0·0135	109·8
$G = 5 \times 10^5$	0·00091	0·00761	113·1	0·0015	0·0149	103·1

(stiffness and mass) of the inner shell are affected by the presence of piezoelectric actuators. As can be seen from these results, a larger control gain can achieve larger reduction of shell vibration and noise transmission. However, the applied electric fields to the piezoelectric actuators exceed the allowable electric field of piezoelectric materials for $G = 5 \times 10^5$. For the actuator located at $x = 0{\cdot}5L$ and $\theta = 60^\circ$, the feedback voltages are 63, 610 and 5084 V, for uniform pressure input, and 108, 356 and 1032 V, for point force inputs with control gains G of 5×10^3, 5×10^4 and 5×10^5, respectively. A voltage requirement of 5084 V would be too large for practical implementation of piezoelectric materials and the results are only included for comparison [40].

The performance of direct velocity feedback is relatively good to control vibrations of the inner shell and a reasonable amount of noise reduction can be achieved when inputs are random point forces. However, for a uniform random pressure input only a modest amount of noise reduction was obtained. In this case, only the modes for which $n = 0$, $m = 1, 3, 5, \ldots$ are present. The efficiency of sound radiation from coupling of these shell modes to acoustic modes is high. Vibration control introduced through localized bending moments from small and discrete pairs of piezoelectric patches do not seem to be very effective for the shell modes which involve uniform stretching around the circumference. Due to practical limitations of the feedback voltage that can be applied to piezoelectric actuators, direct velocity feedback control is not very effective in obtaining a substantial amount of noise reduction for random pressure inputs that are uniformly distributed over the shell surface.

For active control using the sound pressure rate feedback procedure, piezoelectric actuators are assumed to be mounted only on the inner shell. A total number of 270 pairs of actuators is used with the same arrangement as discussed earlier. The pressure sensor (microphone) is located at $x = 3$ m, $\theta = 0^\circ$. Successful application of this approach relies on the design of feasible filters. The modal feedback filters are chosen similarly as in reference [23]:

$$[G_p(\omega)]_{ijk\mu} = -g_p \Psi_{ijk\mu}(x_p, \theta_p, r_p) \sum_{m=1}^{\infty} \sum_{n=0}^{\infty} \sum_{\alpha=0}^{1} Q^p_{mn\alpha} H^{I*}_{mn\alpha} B_{(mn\alpha)(ijk\mu)}, \tag{67}$$

in which g_p is the positive gain of the filter. Substituting equation (67) into equation (56), the acoustic modal active damping factors are

$$\zeta_{ijk\mu} = \sum_{p=1}^{N_{pz}} g_p \Psi^2_{ijk\mu}(x_p, \theta_p, r_p) \left\| \sum_{m=1}^{\infty} \sum_{n=0}^{\infty} \sum_{\alpha=0}^{1} Q^p_{mn\alpha} H^I_{mn\alpha} B_{(mn\alpha)(ijk\mu)} \right\|^2. \tag{68}$$

If the acoustic modal filters are chosen in the form of equation (67), acoustic modal factors from equation (68) are all positive and the solution for interior acoustic pressure is stable. However, these feedback filters need to be determined numerically by solving the *ijkv* simultaneous equations. For a large number of acoustic modes, these solutions require a significant amount of computation time. However, if a single mode or only few modes dominate the acoustic response, simplified expressions could be developed for feedback filters [23].

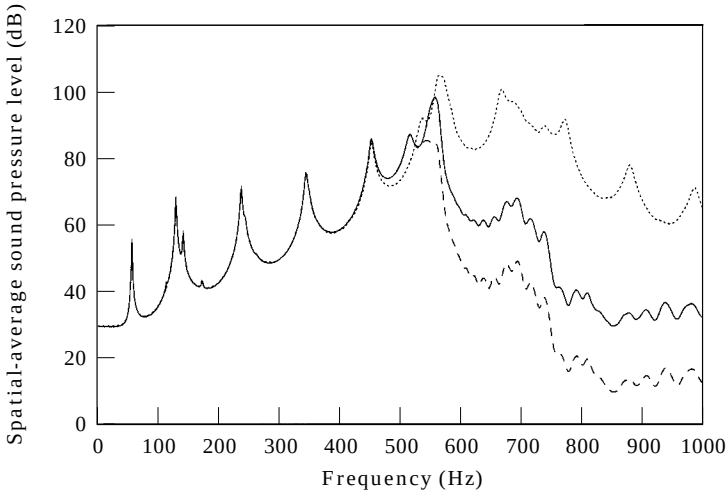

Figure 8. Spatial-average sound pressure levels for uniform pressure with SPL = 110 dB and different control gains: · · · ·, no control; $OASPL_{avg} = 122{\cdot}6$ dB; ——, $g_p = 1 \times 10^4$, $OASPL_{avg} = 110{\cdot}4$ dB; -------, $g_p = 1 \times 10^5$, $OASPL_{avg} = 103{\cdot}5$ dB.

The results presented in Figure 8 are the spatial-average sound pressure levels for several different control gains g_p. These results indicate that a larger gain can achieve a larger amount of noise reduction. The results given in Figure 8 show that active control of noise transmission by the sound pressure rate feedback procedure could be very effective over a significant frequency range. Since piezoelectric actuators are most effective in controlling resonant modal vibrations of the shell, best noise reduction is achieved in the frequency range where both structural and acoustic modes are present. The distinct peaks that appear in Figure 8 in the frequency range of 0–500 Hz are the sound pressure levels at the resonant frequencies of acoustic modes. Since for uniform pressure input no structural modes are excited in this frequency range, active control of shell vibrations by piezoelectric actuators has no significant effect on noise transmission. However, for the chosen interior acoustic conditions, the sound pressure levels at these acoustic resonances do not contribute much to the overall interior sound pressure.

5. SUMMARY AND CONCLUSIONS

The control effectiveness of discrete small piezoelectric actuator patches installed on simply supported double wall composite cylindrical shells subject to random excitation were studied. Direct velocity feedback and sound pressure rate feedback schemes were developed for vibration and noise transmission control. Random sound pressure and random point force inputs were considered. Modal feedback structural and acoustic controlled damping ratios were obtained and their effects were evaluated with respect to: actuator size, electric field gain and

different random input conditions. Theoretical investigations carried out in this study suggest the following:

1. Direct velocity feedback control could provide significant reduction of vibrations for a double wall shell configuration. The discrete piezoelectric actuators are more effective for frequency-ranges of low modal densities.
2. For the chosen geometry and the number of actuators, direct velocity feedback control is not very effective in reducing noise transmission. However, if transmitted noise is dominated by structural shell resonances, velocity feedback control might provide the required levels of noise attenuation.
3. For a double wall configuration, locating active control elements on the inner shell gives more noise reduction than for an equivalent control system located on the outer shell.
4. Increasing the size of discrete actuator patches, increases vibration reduction and transmitted noise attenuation. However, for larger piezoelectric actuators a modal spillover effect was observed.
5. Increasing voltage gain within the acceptable limits of piezoelectric materials could increase actuation capability and decrease vibration and noise levels.
6. The sound pressure rate feedback control is very effective in reducing noise transmission in the frequency range where strong coupling between structural and acoustic modes occurs. However, more research is required to assess the feasibility of this approach for practical implementation: design of modal filters, frequency regions of high structural and acoustic modal densities, shell geometries which represent actual aircraft and other transportation vehicles, realistic random inputs from turbulent boundary layer and powerplant noise, and different geometries of piezoelectric actuators.

In conclusion, discrete pairs of collocated piezoelectric sensors/actuators installed on the shell surface could provide reduction in vibrations and noise transmission. Since the surface area that is covered by these actuators is relatively small in comparison to the total surface area of the shell and the primary action is local bending, their effectiveness in controlling circumferential membrane action dominant modes will be less than those of active lamina layers which cover the entire or large portions of the shell surface [19, 20].

REFERENCES

1. J. C. Stevens and K. K. Ahuja 1991 *AIAA Journal* **29**, 1058–1067. Recent advances in active noise control.
2. G. E. Warnaka 1982 *Noise Control Engineering* **18**, 100–110. Active attenuation of noise—the state of the art.
3. F. W. Grosveld and K. P. Shepherd 1994 *Journal of Aircraft* **31**, 223–227. Active sound attenuation across a double wall structure.
4. A. J. Bullmore, P. A. Nelson and S. J. Elliott 1990 *Journal of Sound and Vibration* **140**, 191–217. Theoretical studies of the active control of propeller induced cabin noise.
5. S. J. Elliott, P. A. Nelson, I. M. Stothers and C. C. Boucher 1990 *Journal of Sound and Vibration* **140**, 219–238. In-flight experiments on the active control of propeller-induced cabin noise.

6. J. V. Warner and R. J. Bernhard 1990 *AIAA Journal* **28**, 284–289. Digital control of local sound fields in an aircraft passenger compartment.
7. C. M. Dorling, G. P. Eatwell, S. M. Hutchins, C. F. Ross and S. G. C. Sutcliffe 1989 *Journal of Sound and Vibration* **128**, 358–360. A demonstration of active noise reduction in an aircraft cabin.
8. R. J. Silcox, H. C. Lester and S. B. Abler 1989 *Journal of Vibration, Acoustics, Stress, and Reliability in Design* **111**, 337–342. Evaluation of active noise control in a cylindrical shell.
9. S. D. Snyder and C. H. Hansen 1994 *Journal of Sound and Vibration* **170**, 443–449. The design of systems to control actively periodic sound transmission into enclosure spaces, part I: analytical models.
10. S. D. Snyder and C. H. Hansen 1994 *Journal of Sound and Vibration* **170**, 451–472. The design of systems to control actively periodic sound transmission into enclosure spaces, part II: mechanisms and trends.
11. D. R. Thomas, P. A. Nelson and S. J. Elliott 1993 *Journal of Sound and Vibration* **167**, 91–111. Active control of the transmission of sound through a thin cylindrical shell, part I: the minimization of vibrational energy.
12. D. R. Thomas, P. A. Nelson and S. J. Elliott 1993 *Journal of Sound and Vibration* **167**, 113–128. Active control of the transmission of sound through a thin cylindrical shell, part II: the minimization of acoustical potential energy.
13. M. A. Simpson, T. M. Luong, C. R. Fuller and J. D. Jones 1991 *Journal of Aircraft* **28**, 208–215. Full-scale demonstration tests of cabin noise reduction using active vibration control.
14. J. D. Jones and C. R. Fuller 1989 *AIAA Journal* **27**, 845–852. Active control of sound fields in elastic cylinders by multicontrol forces.
15. C. R. Fuller and J. D. Jones 1987 *Journal of Sound and Vibration* **112**, 389–395. Experiments on reduction of propeller induced interior noise by active control of cylinder vibration.
16. H. C. Lester and S. Lefebvre 1991 *Proceedings of the Conference on Recent Advances in Active Control of Sound and Vibration*, *Blacksburg*, *VA*, 3–26. Piezoelectric actuator models for active sound and vibration control of cylinders.
17. V. R. Sonti and J. D. Jones 1991 *Proceedings of the Conference on Recent Advances in Active Control of Sound and Vibration*, *Blacksburg*, *VA*, 27–38. Active vibration control of thin cylindrical shells using piezoelectric actuators.
18. C. R. Fuller, S. D. Snyder, C. H. Hansen and R. J. Silcox 1992 *AIAA Journal* **30**, 2613–2617. Active control of interior noise in model aircraft fuselages using piezoceramic actuators.
19. H. S. Tzou, J. P. Zhong and M. Natori 1993 *Journal of Vibration and Acoustics* **15**, 40–46. Sensor mechanics of distributed shell convolving sensors.
20. H.S. Tzou, J. P. Zhong and Hookamp 1994 *Journal of Sound and Vibration* **177**, 63–378. Spatially distributed orthogonal piezoelectric shell actuators (theory and applications).
21. H. S. Tzou, Y. Bao and V. B. Venkayya 1996 *Journal of Sound and Vibration* **197**, 207–224. Parametric study of segmented transducers laminated on cylindrical shells, part 1: sensor patches.
22. H. S. Tzou, Y. Bao and V. B. Venkayya 1996 *Journal of Sound and Vibration* **197**, 225–249. Parametric study of segmented transducers laminated on cylindrical shells, part I: actuator patches.
23. S. Koshigoe, J. T. Gillis and E. T. Falangas 1993 *The Journal of the Acoustical Society of America* **94**, Part 1, 900–907. A new approach for active control of sound transmission through an elastic plate backed by a rectangular cavity.
24. E. F. Crawley 1994 *AIAA Journal* **32**, 1689–1699. Intelligent structures for aerospace: a technology overview and assessment.

25. C. K. Lee 1990 *The Journal of Acoustical Society of America* **87**, 1144–1158. Theory of laminated piezoelectric plates for the design of distributed sensors/actuators, part I: governing equations and reciprocal relationships.
26. E. F. Crawley and J. De Luis 1987 *AIAA Journal* **25**, 1373–1385. Use of piezoelectric actuators as elements of intelligent structures.
27. N. N. Rogacheva 1994 *The Theory of Piezoelectric Shells and Plates*. Boca Raton: CRC Press.
28. H. S. Tzou 1993 *Piezoelectric Shells Distributed Sensing and Control of Continua*. Dordrecht: Kluwer Academic Publishers.
29. E. H. Anderson and N. W. Hagood 1994 *Journal of Sound and Vibration* **174**, 617–639. Simultaneous piezoelectric sensing/actuation: analysis and application to controlled structures.
30. W. Soedel 1993 *Vibrations of Shells and Plates*. New York: Marcel Dekker; second edition.
31. D. A. Bofilios and R. Vaicaitis 1987 *Journal of Aircraft* **24**, 268–273. Response of double-wall composite shells to random point loads.
32. A. E. H. Love 1944 *A Treatise on the Mathematical Theory of Elasticity*. New York: Dover; fourth edition.
33. C.-Y. Wang 1995 *Ph.D. Thesis*, *Columbia University*. Active vibration and noise control of double wall cylindrical shells under random excitation.
34. ANSI/IEEE Std 176–1987 1987 *IEEE Standard on Piezoelectricity*. New York: IEEE.
35. S. W. Tsai 1980 *Introduction to Composite Materials*. Westport: Technomic Publishing.
36. Y. K. Lin 1967 *Probabilistic Theory of Structural Dynamics*. New York: McGraw-Hill.
37. F. P. Mechel 1988 *Journal of the Acoustical Society of America* **83**, 1002–1013. Design charts for sound absorber layers.
38. L. L. Beranek and I. L. Vér (edited) 1992 *Noise and Vibration Control Engineering*: *Principle and Applications*. New York: John Wiley & Sons.
39. R. Haberman 1987 *Elementary Applied Partial Differential Equations*. Englewood Cliffs, NJ: Prentice-Hall; second edition.
40. C. Liang, F. P. Sun and C. A. Rogers 1993 *Smart Structures and Materials* 1993: *Smart Materials* SPIE **1916**, 341–352. Dynamic output characteristics of piezoelectric actuators.

APPENDIX: LIST OF SYMBOLS

E_1, E_2	moduli of elasticity of composite material
G_{12}	shear modulus of composite material
h	thickness
j	$\sqrt{-1}$
k_x, k_θ, k_z	stiffnesses of core
L	length of shell
$M_x, M_\theta, M_{x\theta}$	moment resultants
m	mass per unit area of shell
$N_x, N_\theta, N_{x\theta}$	force resultants
$P_{ijk\mu}$	generalized co-ordinates of sound pressure
Q_θ	out-of-plane shear resultant
R	mean radius of shell
u, v, w	shell displacement components
x, θ, r	cylindrical coordinates
z	shell co-ordinate measured outward from reference surface
v_{12}	Poisson's ratio
ρ	material density
ω_{mn}	natural frequencies of shell

Subscripts and superscripts

a	actuator
b	bonding layer
C	core
E	outer shell
I	inner shell
i, j, k, μ	indices of acoustic modes
m, n, α	indices of shell modes
T	matrix transpose
x	component in longitudinal direction
z	component in transverse direction
θ	component in circumferential direction
*	complex conjugate